C-terminal oligomerization of podocin mediates interallelic interactions

Pál Stráner[1‡], Eszter Balogh[2,3‡] MD, Gusztáv Schay PhD[4], Christelle Arrondel[5], Ágnes Mikó[2,3] MD, Gerda L'Auné[2,3], Alexandre Benmerah PhD[5], András Perczel DSc[1], Dóra K. Menyhárd PhD[1], Corinne Antignac MD, PhD[5,6,7], Géraldine Mollet PhD [5#], Kálmán Tory MD, PhD[2,3,5#*]

[1] MTA-ELTE Protein Modeling Research Group and Laboratory of Structural Chemistry and Biology, Eötvös Loránd University, Budapest, Hungary

[2] MTA-SE Lendület Nephrogenetic Laboratory, Budapest, Hungary

[3] Semmelweis University, I[st] Department of Pediatrics, Budapest, Hungary

[4] Semmelweis University, Department of Biophysics and Radiation Biology, Budapest, Hungary

[5] Laboratory of Hereditary Kidney Diseases, INSERM, UMR 1163, Imagine Institute, Paris, France

[6] Université Paris Descartes-Sorbonne Paris Cité, Imagine Institute, Paris, France

[7] Assistance Publique – Hôpitaux de Paris, Hôpital Necker-Enfants Malades, Département de Génétique, Paris, France

[‡] These authors contributed equally to this work, [#] Co-last authors

Corresponding author:

Kálmán Tory, tory.kalman@med.semmelweis-univ.hu, +36 20 825 8166

Semmelweis University, I[st] Department of Pediatrics, Bókay J. u. 53., Budapest, Hungary, 1083

sources of support: MTA-SE Lendulet Research Grant (LP2015-11/2015), NKFIA/OTKA K109718, K116305, KH125566, MedinProt Synergy grant (DKM, SP and TK), (ANR-10-IAHU-01), EURenOmics (the European Community's 7th Framework program grant 2012-305608), ANR (GenPod project ANR-12-BSV1-0033.01), Eotvos Scholarship (KT), PHC 34501SM Balaton, TeT_14_1-2015-0020

Abstract

Interallelic interactions of membrane proteins are not taken into account while evaluating the pathogenicity of sequence variants in autosomal recessive disorders. Podocin, a membrane-anchored component of the slit diaphragm, is encoded by *NPHS2*, the major gene mutated in hereditary podocytopathies. We formerly showed that its R229Q variant is only pathogenic when trans-associated to specific 3' mutations and suggested the causal role of an abnormal C-terminal dimerization. Here we show by FRET analysis and size exclusion chromatography that podocin oligomerization occurs exclusively through the C-terminal tail (residues 283-382): principally through the first C-terminal helical region (H1, 283-313), which forms a coiled coil as shown by circular dichroism spectroscopy, and through the 332-348 region. We show the principal role of the oligomerization sites in mediating interallelic interactions: while the monomer-forming R286Tfs*17 podocin remains membranous irrespective of the coexpressed podocin variant identity, podocin variants with an intact H1 significantly influence each other's localization (r^2=0.68, P = 9.2 x 10^{-32}). The dominant negative effect resulting in intracellular retention of the pathogenic F344Lfs*4-R229Q heterooligomer occurs in parallel with a reduction in the FRET efficiency, suggesting the causal role of a conformational rearrangement. On the other hand, oligomerization can also promote the membrane localization: it can prevent the endocytosis of F344Lfs*4 or F344* podocin mutants induced by C-terminal truncation. In conclusion, C-terminal oligomerization of podocin can mediate both a dominant negative effect and interallelic complementation. Interallelic interactions of *NPHS2* are not restricted to the R229Q variant and have to be considered in compound heterozygous individuals.

keywords: dominant negative effect, complementation, podocin, nephrotic syndrome, endocytosis, membrane targeting

Introduction

Podocin, named after its podocyte-specific expression, is a member of the stomatin protein family. It is encoded by *NPHS2*, mutations of which are a frequent cause of autosomal recessive steroid-resistant nephrotic syndrome (SRNS) being responsible for 15-39% of congenital and infantile and 13-14% of childhood SRNS.[1-5] Podocin is a 42 kDa integral membrane protein, localized exclusively in the slit diaphragm,[6] with both N- and C-termini facing the cytosolic side.[7] It is associated to lipid rafts where it recruits nephrin through its PHB domain,[6,8,9] thereby augmenting the nephrin-induced activation of the AP-1 transcription factor.[9] In addition, podocin interacts with CD2-associated protein[6], CIN85[10], NOX2[11] and the transient receptor potential C channel protein TRPC6.[12,13] Podocin was found to assemble the NOX2 and TRPC6 complex and thus to allow the gating of TRPC6 by reactive oxygen species.[11] Nevertheless, the function of podocin is not entirely understood. It is known to form oligomers,[6] and all the N- and C-terminal parts and the central PHB domain were shown to homodimerize suggesting that the oligomerization may occur through any of these domains.[8]

The most frequent missense variant of *NPHS2,* R229Q (rs61747728, MAF: 3,75% in Europeans[14]) was formerly found enriched in patients with late-onset focal segmental glomerulosclerosis (FSGS) [15] and to predispose in familial hematuria for high-degree proteinuria[16,17]. We formerly showed that R229Q does not cause FSGS in the homozygous state[18], but only when trans-associated to specific mutations, providing the first example of a clinically determinant interallelic interaction in an autosomal recessive disorder.[19] We found the R229Q podocin to be retained in cytoplasmic compartments by some specific C-terminal missense mutants, as A284V, A288T, R291W, A297V and E310K. We calculated, based on molecular modeling studies, that the R229Q makes the C-terminal helical tail less flexible, which makes it prone to form abnormal heterodimers with these latter podocin mutants also affecting the dimerization. Thus, a potential explanation for the dominant negative effect of these mutants was an altered conformation of their heterodimers with R229Q podocin.[19]

Recently, the 3' frameshift mutation (c.1032delT, p.F344Lfs*4) was also reported to be associated to R229Q in several Kashubian families with SRNS, suggesting it to be the first frameshift mutation pathogenic with R229Q.[20] This prompted us to identify the oligomerization sites of podocin and to investigate how 3' truncating mutations affect the binding capacity and the localization of podocin.

Here we show that oligomerization of podocin occurs exclusively through the C-terminal tail (CTT), and influences the localization of podocin in a complex fashion, mediating either a dominant negative effect or even interallelic complementation.

Results

The C-terminal tail of podocin folds into three helices

The C-terminal part of podocin (residues 124-383) contains a PHB domain (124-282) and a long tail region (CTT, 283-383), the end section of which (distal to N355) is disordered.[21] Three helices are predicted in the CTT (H1-H3) (Fig. 1b).[22] The structure of H1 and H2 were confirmed to be helical both by the crystal structure of stomatin,[23] which shares a homology of 69% in this region with podocin (Fig. 1a,b) and by our previous molecular dynamics simulations.[19] The TVV motif – located in the H2-H3 linker and shown to mediate internalization[24] – is predicted to form a short β-strand (Fig. 1b). In order to assess the role of these regions in the dimerization, we studied the dimerization of three frequent C-terminal frameshift mutants, the R286Tfs*17, the A317Lfs*31, the F344Lfs*4 podocin and a laboratory-derived mutant, the F344* podocin. They all lead to premature stop in the last exon, but they differ in the modular build-up of their CTT domain: while all helical domains are disrupted in the R286Tfs*17 podocin, the H1 remains intact in the A317Lfs*31 podocin, and the F344Lfs*4 or the F344* podocin possesses intact H1, H2 and TVV motifs (Fig. 1c).

Podocin oligomerization occurs exclusively through the CTT

We found an approximately 20% FRET efficiency in the wt and the R229Q homooligomers supporting the formation of strong associations (Fig. 1d,e). In contrast, the FRET efficiency measured between R286Tfs*17 podocin and either the wt or R229Q podocin did not exceed that of the negative control indicating that podocin is unable to dimerize if all three C-terminal helical regions are disrupted (Fig. 1d,e). These results show the exclusive role of the CTT in the oligomerization. The R229Q, A317Lfs*31, F344* or F344Lfs*4 variants markedly influenced the FRET efficiency (Fig. 1d,e), indicating the significant effect of R229Q and the three helical regions on the oligomer conformation.

Figure 1. Podocin dimerizes through the C-terminal tail

a-b) Secondary structure prediction for the C-terminal fragment of stomatin (a) and podocin (b). Wild type C-terminal residues from E210 of stomatin and E264 of podocin are marked according to their loop- (blue), strand- (red) or helix-forming (green) propensity.[22] Values above five indicate significant probabilities. Three helical regions are predicted in both stomatin (H1: 210-244, H2: 245-260, H3: 273-281) and podocin (H1: 283-313, H2: 317-330 and H3: 344-350). The border between H1 and H2 of stomatin is predicted based on the crystal structure of Pyrococcus horikoshii stomatin.[23]

c) Sequence of the studied truncated podocin mutants. The altered sequences following the frameshift sites are framed.

d-e) Förster resonance energy transfer (FRET) efficiency in the oligomers of wt (d) or R229Q podocin (e) and the truncated podocin variants. Wt (d) and R229Q podocin (e) are labeled with the donor dye, the second component by the acceptor dye. As compared with the F344* oligomers, the FRET efficiency increased in the non-pathogenic F344Lfs*4-wt oligomer ($P = 0.0003$) and decreased in the pathogenic F344Lfs*4-R229Q oligomer ($P = 0.024$), showing a different effect of the FDL344_346LTY substitutions on their conformation.

*$P \leq 0.0003$ as compared with the wt-negative control, $^{\#}P \leq 0.006$ as compared with the wt-wt homodimer, $^{\dagger}P = 0.0002$ as compared with the R229Q-negative control, $^{\S}P \leq 0.0003$ as compared with the R229Q-wt dimer, neg.: negative

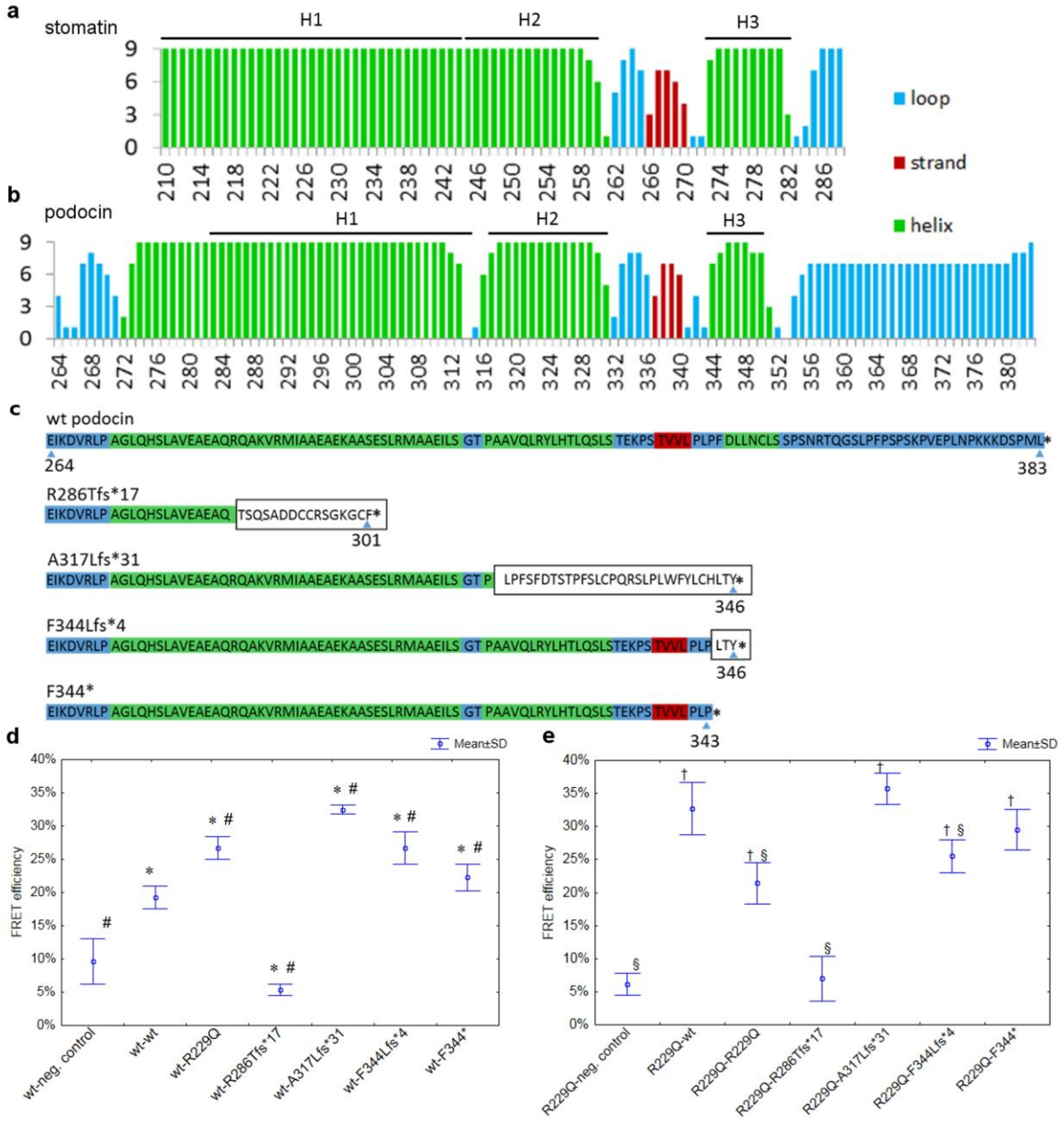
a
stomatin
H1
H2
H3
loop
strand
helix
b
podocin
c
wt podocin
EIKDVRLP AGLQHSLAVEAEAQRQAKVRMIAAEAEKAASESLRMAAEILS GT PAAVQLRYLHTLQSLS TEKPS TVVL PLPF DLLNCLS SPSNRTQGSLPFPSPSKPVEPLNPKKKDSPML*
264
383
R286Tfs*17
EIKDVRLP AGLQHSLAVEAEAQ TSQSADDCCRSGKGCF*
301
A317Lfs*31
EIKDVRLP AGLQHSLAVEAEAQRQAKVRMIAAEAEKAASESLRMAAEILS GT P LPFSFDTSTPFSLCPQRSLPLWFYLCHLTY*
346
F344Lfs*4
EIKDVRLP AGLQHSLAVEAEAQRQAKVRMIAAEAEKAASESLRMAAEILS GT PAAVQLRYLHTLQSLSTEKPS TVVL PLP LTY*
346
F344*
EIKDVRLP AGLQHSLAVEAEAQRQAKVRMIAAEAEKAASESLRMAAEILS GT PAAVQLRYLHTLQSLSTEKPS TVVL PLP*
343
d
Mean±SD
FRET efficiency
wt-neg. control
wt-wt
wt-R229Q
wt-R286Tfs*17
wt-A317Lfs*31
wt-F344Lfs*4
wt-F344*
e
Mean±SD
FRET efficiency
R229Q-neg. control
R229Q-wt
R229Q-R229Q
R229Q-R286Tfs*17
R229Q-A317Lfs*31
R229Q-F344Lfs*4
R229Q-F344*

Podocin oligomerizes through the 273-313 and the 332-348 residues

We subsequently aimed to determine the oligomerization sites of podocin within the CTT, studying homooligomers of C-terminal podocin segments (R168-) with different CTT truncations (Fig. 2). The 168-269 fragment – missing the entire CTT – did not form homodimers according to both FRET analysis and size exclusion chromatography (Fig. 2a,b). Elongation of the sequence just by 17 or 23 amino acids (168-286 and 168-292: containing subsections of the H1 helix) resulted in dimer formation (Fig. 2a), with a low FRET efficiency (Fig. 2b). In contrast, the 168-R286Tfs*17 fragment formed monomers, with low elution volume and no FRET (Fig. 2a,b), similarly to the entire R286Tfs*17 podocin (Fig. 1d,e), indicating that its frameshift sequence disrupts the dimerization. The FRET efficiency of the segment with a full H1 domain (168-313) was already as high as that of the fragment containing all three helical regions (168-348) or the full CTT (168-383), supporting the principal role of H1 in the dimerization (Fig. 2b). The 168-331 sequence, containing both H1 and H2, also formed dimers (Fig. 2a), but exerted a markedly lower FRET (Fig. 2b). This can be explained by our previously built up structural model of the 161-332 podocin homodimer[19]: the PHB domains containing the FRET dye binding sites (Suppl. Fig. 1), are 60 Å apart, near the limit of FRET detectability. The higher FRET efficiency of the 168-313 homodimer suggests a slight rotation of the interacting helices which create in a 10-15 Å shift of the PHB domains (Fig. 2c). Once the segment contained all three CTT helices (168-348 or 168-383), the presence of high order oligomers (Fig. 2a) was also detected. These results show that the second oligomerization site is located in the region of the 332-348 residues building up the H2-H3 linker and the H3 helix.

Figure 2. Oligomerization sites of podocin

a-b) Homooligomerization capacity of MBP-fused C-terminal podocin fragments assessed by size exclusion chromatography (a) and FRET analysis (b). The fragment without the H1 helix (168-269) and the fragment corresponding to the R286Tfs*17 mutant (168-286fs) formed monomers according to both analyses. Fragments containing at least the first part of H1 (168-286), (168-292), the entire H1 (168-313) or also the H2 (168-331) formed dimers (a) with a variable FRET efficiency (b). The fragment containing also the H2-H3 linker (168-348) and the full CTT formed also oligomers (a) and produced highly efficient FRET (b).

*, **, *** levels of significance as compared with the FRET efficiency of the 168-269 fragment: $*P = 0.034$, $**P \leq 0.004$, $***P = 0.0002$, $^{\#}P = 0.0002$ as compared with the FRET efficiency of the full CTT (168-383)

c) Probable arrangements of various podocin fragments in stable homodimers, created based on our previously published dimer model. Models are colored according to the chromatograms of a), the labeled Cys254 residues are shown in yellow. The Cys254(monomerA)-Cys254(monomerB) separation increases due to the partial absence of H1 (in case of R168_R286 and R168_M292) or the joint presence of H1 and H2 (R168_S331), compared with a dimer containing only the entire H1 helix (R168_S313) with more optimal Cys254(monomerA)-Cys254(monomerB) separation.

d) Far-UV ECD spectra of the H1 domain (P271_S313) from 5°C to 65°C, showing the presence of an α-helical structure at low temperatures, which is unfolded by heating.

e) The ratio of molar ellipticity at 222 and 208 nm of the H1 domain (P271_S313), as a function of the temperature between 5°C and 85°C, reflects a coiled-coil association. After cooling, the spectra of an α-helical coiled coil structure could be recovered.

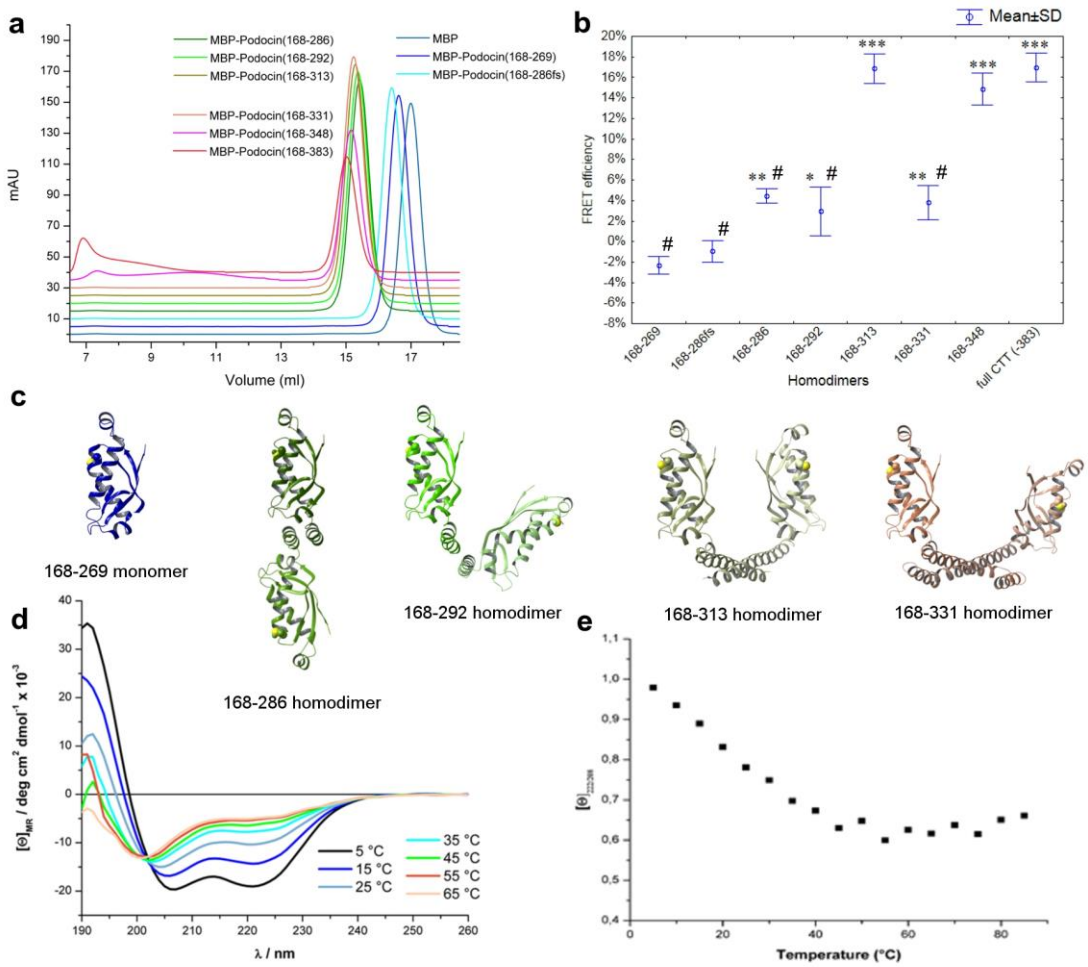
a
MBP-Podocin(168-286)
MBP-Podocin(168-292)
MBP-Podocin(168-313)
MBP-Podocin(168-331)
MBP-Podocin(168-348)
MBP-Podocin(168-383)
MBP
MBP-Podocin(168-269)
MBP-Podocin(168-286fs)
mAU
Volume (ml)
b
Mean±SD
FRET efficiency
168-269
168-286fs
168-286
168-292
168-313
168-331
168-348
full CTT (-383)
Homodimers
c
168-269 monomer
168-286 homodimer
168-292 homodimer
168-313 homodimer
168-331 homodimer
d
5 °C
15 °C
25 °C
35 °C
45 °C
55 °C
65 °C
λ / nm
e
Temperature (°C)

Supplementary Figure 1. Position of the cysteine residues in the 168-348 podocin fragment

The two cysteine residues in the 168-348 segment, Cys193 and Cys254, are both located in the PHB domain. Since the Cys193 points toward the inner core of the domain, the Cys254 residue is the expected maleimide binding site.

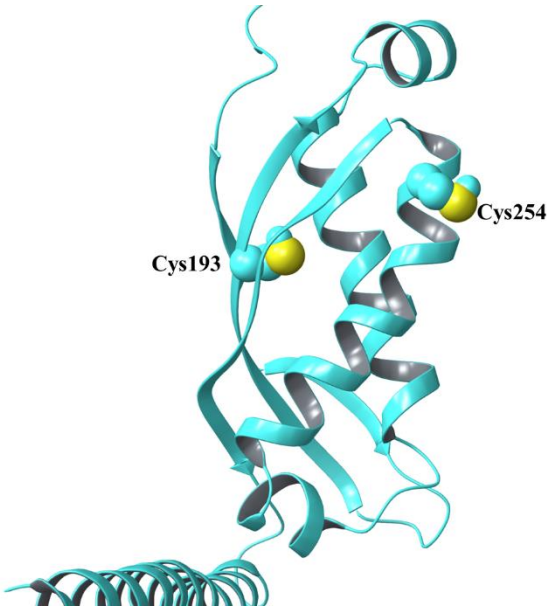

The H1 domain forms coiled-coil like associations

We assessed the structure of the first oligomerization site by measuring its temperature-dependent far-UV ECD spectra (Fig. 2d). At 5°C the ECD spectrum displayed a positive maximum near 190 nm and two minima at 208 and 222 nm with a 222/208 nm ellipticity ratio characteristic of coiled-coil alpha-helices. [25] Above 40°C, the unstructured propensity increased, indicating the emergence of a structural ensemble of elevated internal dynamics, with the ellipticity ratio decreasing below 0.7. This effect was reversible: the ECD spectrum regained its former characteristics typical of coiled-coil alpha-helices after cooling back from 85°C to 5°C. These findings confirm that the first oligomerization site reversibly forms coiled-coil like associations (Fig. 2d,e).

Effect of C-terminal truncation on the localization

The C-terminal truncations led to markedly different localization: while we found the R286Tfs*17 podocin to be as membranous as the wt podocin, the A317Lfs*31 podocin was only partly membranous and the F344Lfs*4 and F344* podocin mutants localized in vesicles (Fig. 3a). The perfect membranous localization of R286Tfs*17 is in accordance with its hypomorphic nature, as patients who are either homozygous for R286Tfs*17 or carry a null mutation in trans, progress to ESRD at the median age of 14 years (range: 8-17, *n* = 13) in the French cohort, i.e. later than patients with the A317Lfs*31 mutation (median: 6.2, range: 3.9-11, *n* = 6, *P* = 0.02), or compared to patients with two null mutations.[26]

Figure 3. Membrane targeting of podocin variants as a function of the coexpressed podocin variant

a) Podocytes expressing GFP-tagged wt and missense podocin variants and/or HA-tagged wt and truncated podocin variants. The GFP-tagged podocin variants are shown in green, the HA-tagged podocin variants are in red. The plasma membrane is labeled with wheat germ agglutinin and shown in blue. The R286Tfs*17 podocin is perfectly membranous, does not colocalize with any of the coexpressed podocin variants, nor is influenced in its localization by them (c). In contrast, the A317Lfs*31 podocin is only partially membranous and the F344* and F344Lfs*4 podocin variants localize in vesicles. These three podocin variants colocalize with the coexpressed podocin variants and are strongly influenced in their localization by them (c, Suppl. Fig. 2). Interestingly, the F344* and F344Lfs*4 podocin mutants become perfectly membranous when associated with membranous podocin variants, except for the pathogenic R229Q-F344Lfs*4 association. This latter shows a dispersed reticular localization, typical of pathogenic R229Q-associations. Scale bar, 20µm.

b-c) Membrane targeting of GFP-tagged missense and wt podocin variants (b) and HA-tagged truncated and wt podocin variants (c) as a function of the coexpressed podocin variants shown in parentheses, quantified in 10 cells per group. *P* values show the significance of Kruskal-Wallis tests.

*, **, *** levels of significance as compared with the membrane localization of the corresponding monoexpressed variant: *$P \leq 0.05$, **$P = 0.002$, ***$P \leq 0.0001$

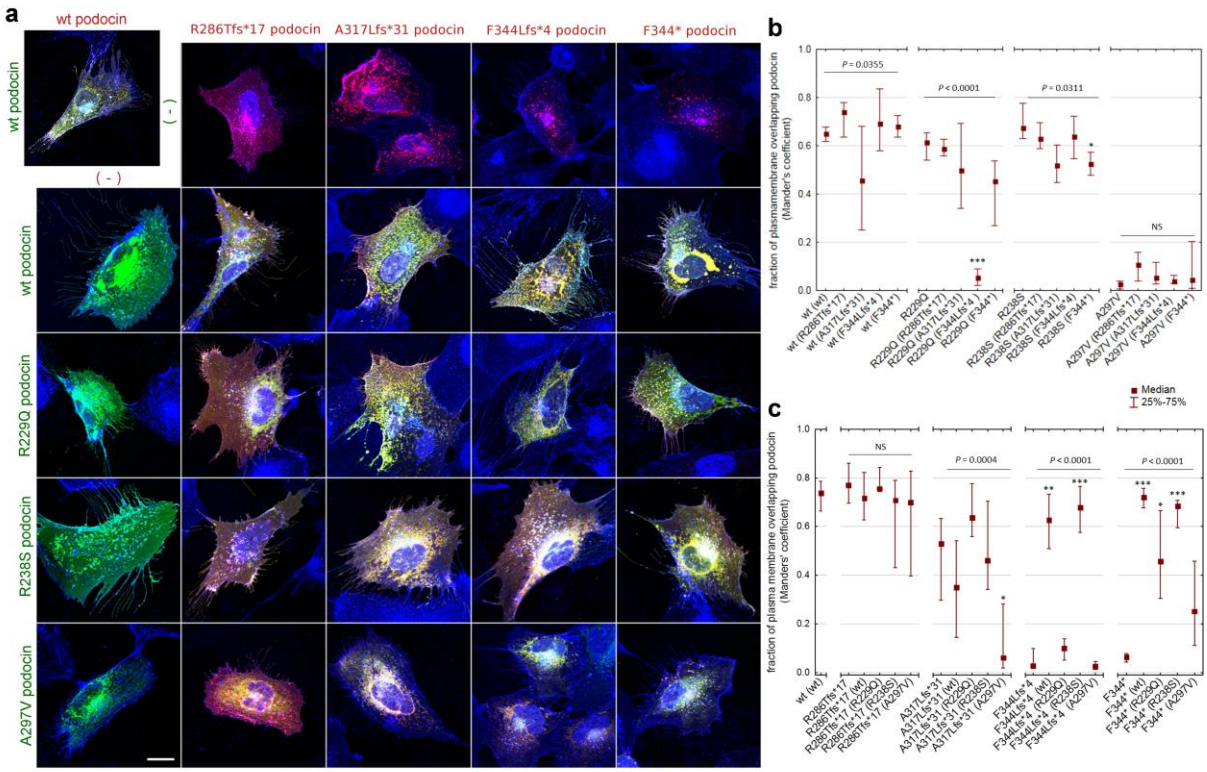

Supplementary Figure 2. Correlation in the membrane localization of coexpressed podocin variants between variants with (a, c) and without (b, d) dimer-forming capacity. (suppl. to Fig. 3)

Data are presented either as the values obtained in single cells (a,b) or as a median calculated in each group of 10 cells expressing the same podocin pairs, corresponding to Figure 3. While there is a strong correlation in the membrane-localization of the coexpressed podocin variants forming heterodimers or heterooligomers (a,c), the correlation in the membrane localization of podocin variants which do not form heterodimers is weak (b) or absent (d).

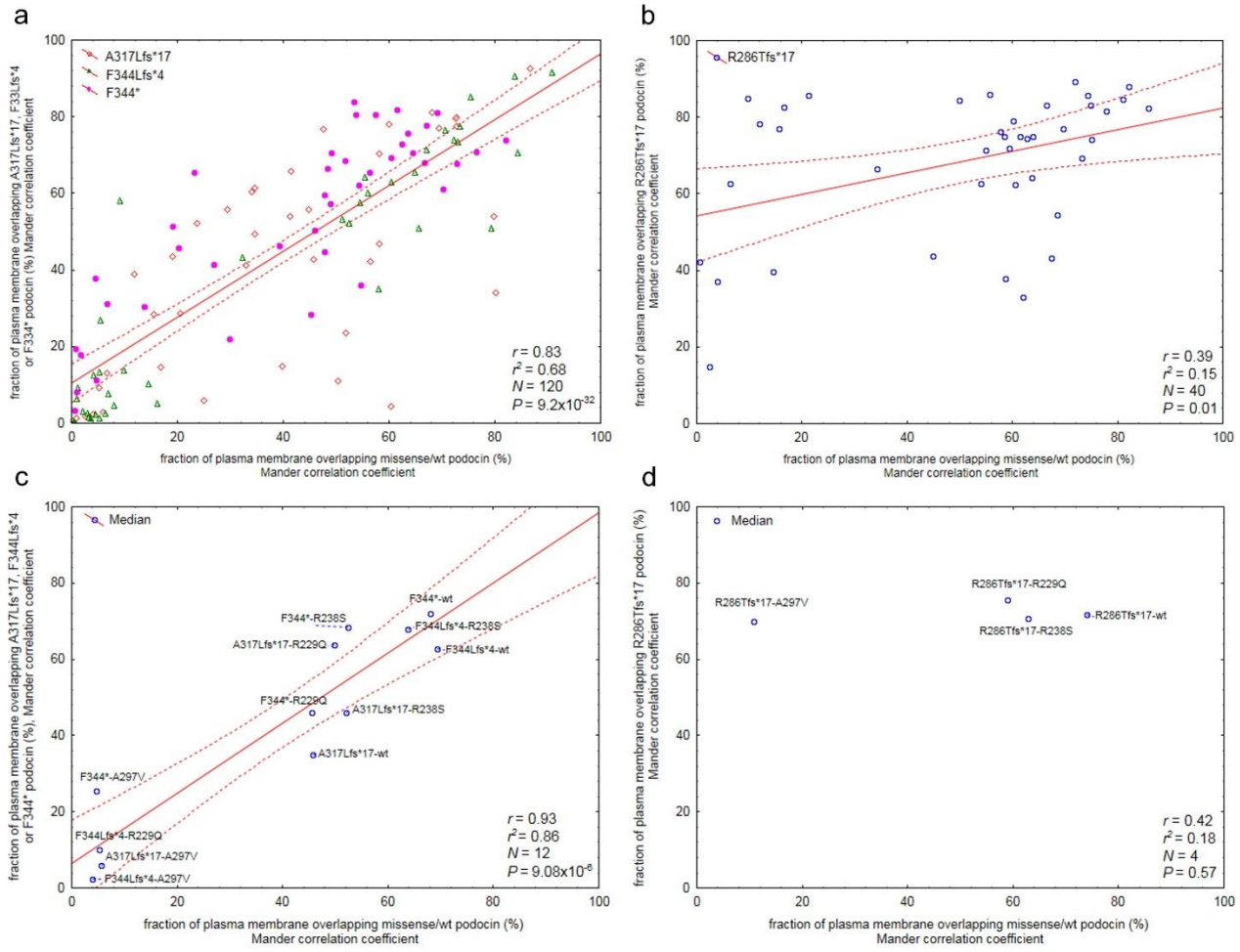

The F344Lfs*4 and F344* mutations result in internalization of podocin

The distinct vesicular localization of the F344Lfs*4 and F344* podocin variants suggested their internalization, in accordance with former results.[24] We found indeed vesicles positive for both internalized transferrin and F344Lfs*4 and F344* podocin variants supporting their clathrin-mediated endocytosis (Fig. 4a). Furthermore, blocking the dynamin-mediated endocytosis by coexpressing the dominant negative mutant (K44A) dynamin,[27] made the F344Lfs*4 and F344* podocin variants partially membrane-localized (Fig. 4b,c). These results showed that the vesicular localization of the F344Lfs*4 and F344* podocin variants is at least partially due to endocytosis (Fig. 5).

Figure 4. The F344Lfs*4 and F344* podocin mutants are internalized

a) The HA-tagged F344Lfs*4 podocin and the fluorescent transferrin, internalized for 10 minutes, colocalize in vesicles of podocytes, suggesting that F344Lfs*4 podocin is endocytosed. Scale bar, 20µm.

b) Blockade of endocytosis by the coexpression of dominant negative (K44A) dynamin makes the F344Lfs*4 and F344* podocin variants partially membranous. HA-tagged podocin variants or transferrin are shown in red, GFP-tagged dynamin in green and WGA or Hoechst in blue. While endocytosis was not altered by wt dynamin, it was inhibited by K44A dynamin with a dominant negative effect, as demonstrated by the lack of transferrin uptake in the cell expressing K44A dynamin. K44A dynamin makes the F344Lfs*4 and F344* podocin variants partially membranous (c), indicating that their vesicular localization is explained at least partially by internalization. Scale bar, 20µm.

c) Membrane targeting of podocin as a function of the coexpressed dynamin variant, quantified in 10-12 cells per group.

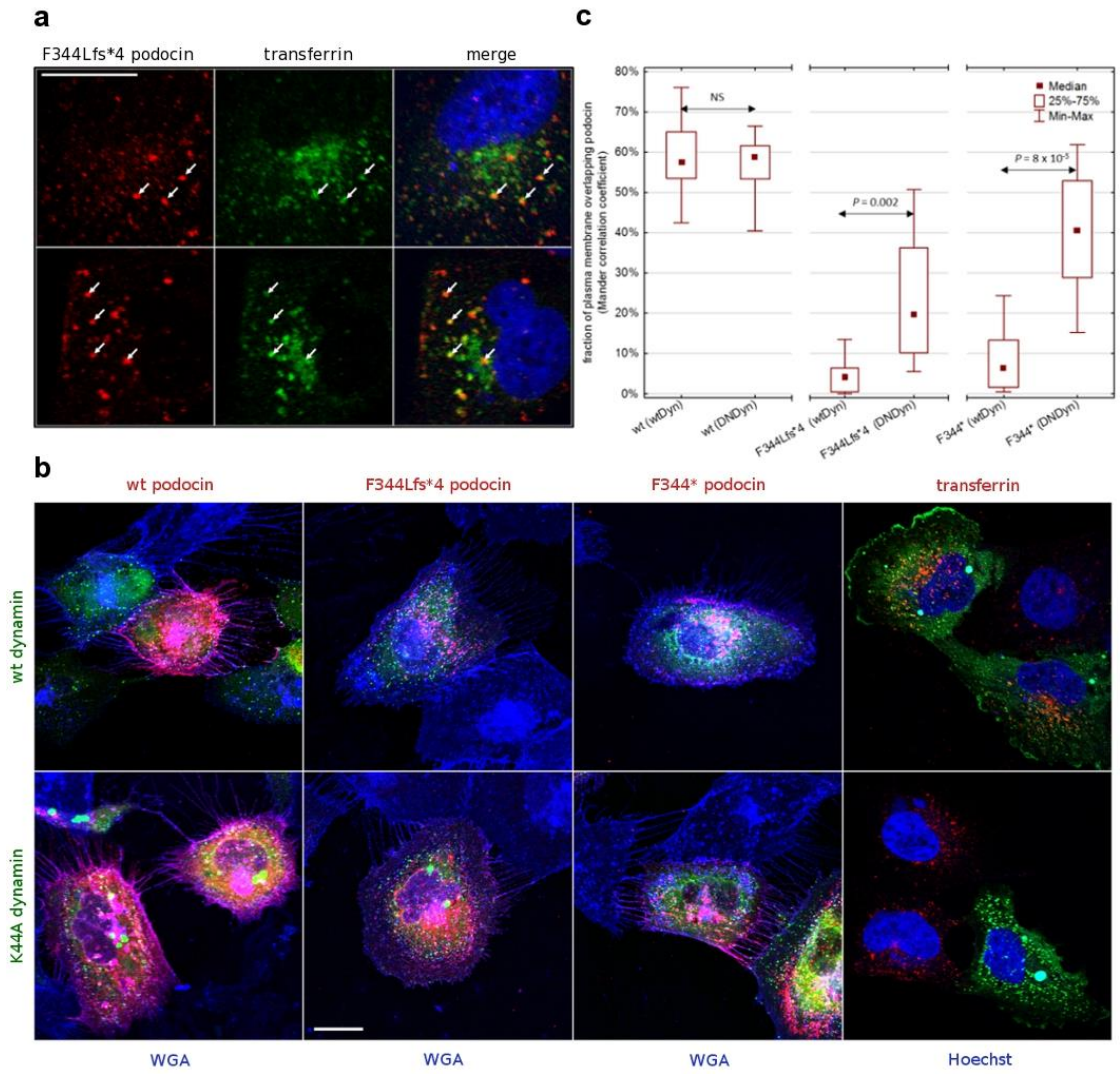
a
F344Lfs*4 podocin
transferrin
merge
c
fraction of plasma membrane overlapping podocin (Mander correlation coefficient)
80%
70%
60%
50%
40%
30%
20%
10%
0%
NS
P = 0.002
P = 8 x 10-5
Median
25%-75%
Min-Max
wt (wtDyn)
wt (DNDyn)
F344Lfs*4 (wtDyn)
F344Lfs*4 (DNDyn)
F344* (wtDyn)
F344* (DNDyn)
b
wt podocin
F344Lfs*4 podocin
F344* podocin
transferrin
wt dynamin
K44A dynamin
WGA
WGA
WGA
Hoechst

F344Lfs*4 podocin retains R229Q podocin in accordance with their pathogenicity

We next investigated the localization of R229Q podocin as a function of the coexpressed truncated podocin variants. As the allele frequency of R229Q (3.8% in Europe) is 50x higher than the cumulative allele frequency of all other pathogenic *NPHS2* variants in the European population,[14] the pathogenicity of its associations with relatively frequent mutations can be judged on an epidemiological basis.[19] Among the truncating mutations, F344Lfs*4 has been uniquely reported to be frequently associated to R229Q in patients,[5,20,28] rendering the pathogenicity of their association unquestionable. On the other hand, A317Lfs*31 and R286Tfs*17 are unexpected to be pathogenic with R229Q, either because they have never been associated to R229Q in affected individuals despite their high allele frequency in the patient cohorts (A317Lfs*31) or were associated to R229Q in patients with steroid-sensitive nephrotic syndrome (R286Tfs*17) proving the functionality of R229Q podocin when coexpressed with R286Tfs*17 podocin.[29] Along this line, R229Q podocin lost its membrane localization only when coexpressed with F344Lfs*4 (Fig. 3a,b, Fig. 5), with a similar dispersed reticular localization to that of the other pathogenic associations of R229Q.[19] As the F344* podocin did not abolish the membrane localization of R229Q podocin, the dominant negative effect of F344Lfs*4 is expected to be exerted by the FDL344_346LTY substitutions and not by the C-terminal truncation (Fig. 3a,b).

In accordance with the recessive transmission of *NPHS2*-associated nephrotic syndrome, the wt podocin remained membranous when coexpressed with all four truncated podocin variants, though A317Lfs*31 decreased its membrane-targeting in a non-significant, highly variable fashion (Fig. 3a,b). Furthermore, unexpectedly, the wt podocin made the coexpressed F344Lfs*4 or F344* podocin mutants perfectly membranous, suggesting a complementary effect (Fig. 3a,c, Fig. 5). This prompted us to examine the effect of missense podocin mutants on the localization of the truncated podocin variants.

Missense podocin variants can restore the membrane localization of the truncated forms

In addition to the wt and R229Q podocin, we coexpressed the R238S and A297V podocin variants with the truncated podocin proteins to study their interactions. While the R238S podocin has an intact CTT domain and is known to be membranous (Fig. 3a,b),[30] the A297V podocin has an altered CTT structure [19] and shows a dispersed reticular localization (Fig. 3a,b).

In accordance with the lack of its dimerization capacity, the R286Tfs* podocin did not colocalize with any of the coexpressed podocin variants through their trafficking (Fig. 3a), and the membrane localization of R286Tfs* podocin was not influenced by any of them (Fig. 3a,c, Fig. 5, Suppl. Fig. 2).

The truncated podocin variants with an intact H1 domain (A317Lfs*31, F344Lfs*4 and F344*) strongly colocalized with the missense mutants, and their localization was significantly influenced by them (Fig. 3a,c, Suppl. Fig. 2). They showed a dispersed reticular localization when coexpressed with A297V podocin (Fig. 3a), similar to that of the R229Q-A297V association.[19] Thus, A317Lfs*31 podocin lost its partial membrane localization with A297V podocin. On the other hand, the R238S podocin, similarly to the wt podocin, made the F344Lfs*4 and F344* podocin variants perfectly membranous (Fig. 3a,c). Along the same line, the R229Q podocin exerted a similar complementary effect on the localization of F344* podocin, indicating that missense podocin variants can block the internalization of coexpressed truncated podocin mutants. The effect of the C-terminal truncations on the podocin localization and the pathogenicity of different associations is summarized in Fig. 5.

Figure 5. Degree of oligomerization, localization and pathogenicity of truncated podocin associations.

Both the wild type and R229Q oligomers (a) and the R286Tfs*17 monomers (b) are targeted to the plasma membrane. The pathogenic R229Q heterooligomers (here R229Q-F344Lfs*4) are localized in intracellular vesicles (c). Podocin variants lacking the region downstream to residue 343 are internalized (d), unless they heterodimerize with a membranous podocin variant with an intact C-terminal tail (e).

[#]predicted on an epidemiological basis, [†]predicted based on the localization of F344Lfs*4 podocin.

wt podocin is shown in (light and dark) blue, R286Tfs*17 podocin in orange, R229Q podocin in purple, F344Lfs*4 in (dark and light) green

nuc: nucleus, ER: endoplasmic reticulum, NS: nephrotic syndrome, ref: reference

genotype	predicted degree of oligomerization	localization (type on the diagram)	clinical pathogenicity (ref)
[wt];[wt]	homooligomers	membranous (a)	benign
[wt];[R229Q]	heterooligomers	membranous (a)	benign
[R229Q];[R229Q]	homooligomers	membranous (a)	benign (18)
[R286Tfs*17];[R286Tfs*17]	monomers	membranous (b)	intermediate-onset NS
[R286Tfs*17];[wt]	R286Tfs*17 monomer	membranous (b)	benign
	wt oligomers	membranous (a)	
[R286Tfs*17];[R229Q]	R286Tfs*17 monomer	membranous (b)	benign (29)
	R229Q oligomers	membranous (a)	
[A317Lfs*31];[A317Lfs*31]	homodimers	partially membranous	early-onset NS (26)
[A317Lfs*31];[wt]	A317Lfs*31 homodimers	partially membranous	benign
	heterodimers	partially membranous	
	wt oligomers	membranous (a)	
[A317Lfs*31];[R229Q]	A317Lfs*31 homodimers	partially membranous	benign[#]
	heterodimers	membranous	
	R229Q oligomers	membranous (a)	
[F344Lfs*4];[F344Lfs*4]	homooligomers	internalized (d)	early-onset NS[†]
[F344Lfs*4];[wt]	heterooligomers	membranous (e)	benign
[F344Lfs*4];[R229Q]	heterooligomers	intracellular reticular/vesicular (c)	adult-onset FSGS (20)

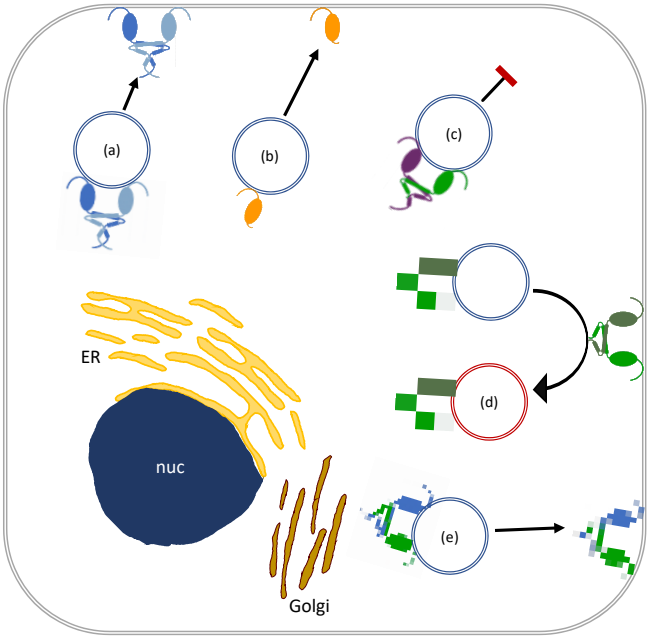

Discussion

We formerly predicted that the C-terminal heterodimerization can mediate a dominant negative effect, and thus plays a key role in determining the pathogenicity of *NPHS2* R229Q, the most common variant implicated in podocytopathies.[19] Here we supply experimental data on the podocin dimerization, identify the oligomerization sites and present a novel mechanism through which coexpressed podocin variants can influence the localization of each other.

We found podocin to oligomerize exclusively through the C-terminal tail, as the R286Tfs*17 podocin, with all three C-terminal helixes disrupted, is unable to dimerize, and, accordingly, does not colocalize through the trafficking with coexpressed podocin variants. This contrasts with the previously found capacity of the N-terminal region and the PHB domain to homodimerize, as shown by coimmunoprecipitation.[8] This controversy is partially explained by our finding that the 270-286 residues, belonging mainly to the PHB domain (124-282) and helical after the A272 residue can already mediate dimerization. We found the R286Tfs*17 to be a membranous and hypomorphic mutation, potentially explained by its intact PHB domain and thus reserved nephrin binding capacity.[8] These results show that podocin dimerization is not necessary neither for membrane-targeting, nor for a partial function. Stomatin oligomerization is similarly mediated by the C-terminal, but not by the N-terminal region [31,32], and is not prerequisite for membrane-targeting either.[32]

Within the CTT, we found the oligomerization to be mediated by the 273-313 residues, corresponding primarily to the H1 domain and by the 332-348 residues, corresponding to the H2-H3 linker and H3 helix. The H2 helix also influenced the dimerization though did not mediate it directly. In accordance with our previous molecular dynamics simulations,[19,23] here we supplied experimental support for the coiled coil structure of the first oligomerization site by CD spectroscopy, providing the first direct data on the structure of a podocin fragment. These results are in perfect accordance with the organization of stomatin in homo-oligomeric complexes – comprising of 9- to 12-mers [31] – by the interaction of its coiled coil region,[32] corresponding to H1 in podocin, and the 265_273STIVFPLPI residues,[33] corresponding to the 336_344STVVLPLPF region of podocin. We found the podocin to

oligomerize *in vitro* showing that raft-association is not necessary for its oligomerization. Furthermore, podocin fragments expressed in bacteria and in human cells produced a similar FRET efficiency, making it unlikely that eukaryote-specific post-translational modifications are required for oligomerization.

Several observations demonstrate the causal relationship between oligomerization and interallelic interactions. We found the membrane localization of coexpressed podocin variants to strongly correlate only when the coexpressed podocin variants were able to dimerize. Furthermore, the H1, H2 and H3 regions correspond to the localization of the mutations that have been found pathogenic in trans with R229Q (H1: A284V, A288T, R291W, A297V, E310K, H2: L327F and Q328R, H3: F344Lfs*4).[19] Finally, the FDL344_346LTY substitutions of F344Lfs*4 podocin exerted a dominant negative effect on R229Q podocin and changed in parallel the conformation of their heterodimer, as reflected by a decreased FRET efficiency.

The oligomerization sites of podocin provide an explanation as to why the F344Lfs*4 podocin and not the R286Tfs*17 or A317Lfs*31 podocin mutants are pathogenic with R229Q even though all three affect oligomerization sites. The R286Tfs*17 podocin does not even dimerize with R229Q podocin. Though the A317Lfs*31 podocin binds it strongly and contains several substitutions that are known to induce formation of pathogenic oligomers with R229Q podocin (L327F or FDL344_346LTY), it lacks both the H2 and the second oligomerization site. The A317Lfs*31 podocin is thus expected to form only dimers, providing a potential explanation for its insufficient R229Q-retaining capacity.

Besides the dominant negative effect, we found that oligomerization can mediate another type of interallelic interaction. In accordance with the results of Godel et al,[24] who showed that a C-terminal truncation distal to the TVV337-339 motif leads to internalization, we found both the F344Lfs*4 and the F344* podocin mutants to be endocytosed. Their colocalization with internalized transferrin and partial membranous localization when coexpressed with the dominant negative mutant dynamin,[34] suggest that their endocytosis is clathrin-mediated, in accordance with recent data.[35] Excitingly, these mutants became membranous when coexpressed with membranous podocin variants with an

intact CTT. As such, the coexpression of R238S podocin prevented the endocytosis of F344Lfs*4 podocin providing the first example of a complementation between two pathogenic *NPHS2* mutations. It therefore seems to be sufficient for one component of the oligomer to contain an intact C-terminal to prevent endocytosis.

It is tempting to speculate that the restored membrane localization of F344Lfs*4 podocin allows its partial functioning, in agreement with the hypomorphic nature of all membranous podocin mutants: the V180M, R238S or V290M podocin,[30,36,37] or even the R286Tfs*17 podocin which lacks the whole CTT. Whether these hypomorphic mutations can entirely complement each other's function remains to be determined. Interestingly, not a single patient compound heterozygous for them has ever been published.[36,38] In accordance with the principal role of C-terminal oligomerization in the interallelic interactions, a *de novo* dominant *NPHS2* mutation, segregating over three generations with the diseased phenotype (c.988_989delCT, p.L330Vfs*15) and affecting the second oligomerization site, has been recently published.[39] This indicates that the wild type podocin can also be the subject of a dominant negative effect, as suggested by the reduced membrane targeting of wt podocin in the presence of A317Lfs*31 podocin in our experiments as well. These results emphasize that the interallelic interactions of *NPHS2* are not restricted to the R229Q variant. Therefore, while evaluating the pathogenicity of 3' *NPHS2* mutations, interallelic interactions have to be taken into account. A C-terminal truncating mutation is expected to exert a dominant negative effect if it does not disrupt the oligomerization, i.e. causes amino acid substitutions only in the second oligomerization site leading to a conformational rearrangement of the oligomer. Such an *NPHS2* mutation leads to premature stop codon in the last exon and therefore does not result in nonsense-mediated RNA decay. The dominant negative effect is however also dependent on the trans-associated variant: while the L330Vfs*15 mutation is known to be pathogenic in trans with the wt allele, the F344Lfs*4 is only pathogenic with R229Q. Interallelic interactions influencing the degree of pathogenicity of trans-associated pathogenic variants have been described in enzymopathies.[40,41] The interactions of *NPHS2*

are nevertheless the first in an autosomal recessive disorder which act through the membrane-trafficking and can invert the non-pathogenic nature of a variant.

In conclusion, podocin oligomerization occurs through two C-terminal sites. Though it is not prerequisite for the membrane-localization, it can mediate interallelic interactions in several ways. In addition to the dominant negative effect, it can also result in complementation. These interactions therefore have to be considered while evaluating the pathogenicity of trans-associated 3' *NPHS2* variants in compound heterozygous individuals.

Methods

Generation of podocin-coding plasmids

Human wild type podocin cDNA was amplified from the constructs described by Roselli et al [42] and subcloned into the BamHI/XhoI sites of LentiORF pLEX-MCS (Open Biosystems) or in frame with the Green Fluorescent Protein (GFP) cDNA into the XhoI/EcoRI sites of pEGFP-N1 (Clontech). The mutations R229Q, R238S, A297V, R286Tfs*17, A317Lfs*31, F344Lfs*4 and F344* were created using the QuickChange Site-directed Mutagenesis kit according to the manufacturer's instructions (Agilent). Two copies of the hemagglutinin (HA) epitope tag were inserted by mutagenesis in the pLEX-MCS-podocin construct to express N-terminal HA-tagged proteins.

For bacterial expression, the malE gene of pMAL-c2x and the GST gene of pGEX4T1 were cloned into the NdeI/BamHI sites of pET32b vector. The constructs encoding the 168-269, 168-286, 168-R286Tfs*17, 168-292, 168-313, 168-331, 168-348 and 168-383 C-terminal fragments of podocin were subsequently cloned into the pET32b_MBP vector, the H1 fragment (272-313) into the pET32b_GST vector as an BamHI/XhoI DNA fragment. Constructs were verified by Sanger sequencing.

Fluorescence Spectroscopy

Podocin variants were expressed in HEK293 cells, cultured at 37°C in DMEM, high glucose with 10% FBS and 1% Penicillin-Streptomycin (Gibco, Thermo Fisher Scientific). Mycoplasma contamination was tested every month. Cells were transfected with vectors encoding HA-tagged podocin variants (CalPhos Mammalian Transfection Kit, Clontech). Transfected cells were incubated for 48 hours and lysed by 150 mM NaCl, 20 mM Tris, 1% Triton-X supplemented with 0.1% protease inhibitor (Protease Inhibitor Cocktail, Sigma Aldrich). Lysis and upcoming procedures were performed on ice. Lysates were incubated with monoclonal anti-HA antibodies (clone HA-7, Sigma Aldrich) and subsequently with Protein G magnetic beads (Dynabeads Protein G for Immunoprecipitation, Thermo Fisher Scientific). Immunprecipitates were washed three times with lysis buffer. Podocin variants were eluted by competition with HA peptides (HA Peptide lyophilized powder, Biotool), five times,

each elution lasting at least 30 minutes. Concentration of the eluates was measured by spectrophotometry (DC Protein Assay, Bio-Rad). Eluates were verified by SDS-PAGE. Ten μg protein was loaded on 4–20% MiniPROTEAN® TGX StainFree™ Protein Gel and transferred to a Trans-Blot® Turbo™ Mini Nitrocellulose membrane (Bio-Rad). Membranes were blocked with 5% nonfat dry milk in PBS and were incubated with anti-HA as primary (clone HA-7, Sigma Aldrich in PBS- 0.1% Tween 20) and goat anti-mouse IgG-HRP as secondary antibodies (sc-2005, Santa Cruz Biotechnology). Proteins were visualized by chemiluminescence (Western Blotting Luminol Reagent, sc-2048, Santa Cruz Biotechnology) on Molecular Imager VersaDoc MP 5000 System (Bio-Rad).

Protein aliquots (0.4 nmol) were stained separately with 4 nmol of either Alexa Fluor 488 C5 Maleimide (donor dye) or Alexa Fluor 555 C2 Maleimide (acceptor dye) molecules (Invitrogen, Thermo Fisher Scientific) and were incubated overnight at 4°C. Differently stained podocin variants were subsequently mixed two by two for oligomerization, incubated for 2 hours on RT and washed through PD SpinTrap G-25 filter column (GE Healthcare Sciences) to discard the unbound HA peptides and fluorophores. Förster type Resonance Energy Transfer (FRET) was measured between two differently stained podocin variants in a final volume of 100 μl, containing each podocin with a concentration of 4 μM. The fluorescence lifetime of the donor dye (Alexa 488 C5) was measured with a Chronos BH Time Correlated Single Photon Counting lifetime spectrometer (ISS Inc., Champaign, IL) using an excitation wavelength of 488 nm with a 3 nm band pass and an emission wavelength of 524 nm with a 5 nm band pass. A pulsed excitation of 0.8 ns full width at half maximum was used and 3 x 10^8 pulses were integrated for each lifetime measurement. The fluorescence lifetime was determined by an iterative re-convolution procedure employing least-squares fitting using the Vinci2 software (ISS Inc). Every iterative re-convolution was repeated at least three times with different starting parameters set to ensure correct convergence of the fitting parameters. The lifetime was determined both by multi-exponential fitting, and by lifetime distribution fitting. The variance (Var) of the lifetime values was determined from the nonlinear least squares algorithm by $Var(\tau) = \sigma^2 \cdot \nabla f(\tau) * \nabla f(\tau)^T$ where τ is the fitted lifetime parameter set, $\nabla \mathbf{f}$ is the gradient vector of the fitting

function, and σ^2 is the chi-square error value. The FRET efficiency is computed as $FRET = 1 - \frac{\tau_{sample}}{\tau_{donor}}$ where τ_{sample} is the donor dye lifetime in the donor-acceptor pair sample, and τ_{donor} is the donor dye lifetime without acceptor present. The standard deviation of the FRET values was determined from the variances by the Taylor-expansion method according to the equation: $\mathrm{Var(FRET)} = \mathrm{Var}(\tau_{\mathrm{donor}}) \cdot \left(\frac{\partial FRET}{\partial \tau_{donor}}\right)^2 + Var(\tau_{sample}) \cdot \left(\frac{\partial FRET}{\partial \tau_{sample}}\right)^2$. Experiments were repeated three times on samples obtained from at least two different expressions. The FRET efficiency values were averaged, and the standard deviation was calculated according to the summation rule of the variances assuming the independency of the measurements.

Expression and purification of podocin fragments in E. coli

Bacteria (*E. coli* strain BL21-DE3) were transformed and grown at 37°C in LB media supplemented with 100 µg/ml ampicillin and 2 g glucose to the OD600 of 0.8. To induce protein expression, 0.25 mM isopropyl b-D-1-thiogalactopyranoside (IPTG) was added. After 18 hours of incubation at 16°C, cells were harvested by centrifugation (4500 x g, 20 min, 4°C).

Pelleted cells containing the GST-fused H1-fragment were resuspended in buffer A (50 mM Tris, 150 mM NaCl, 1 mM EDTA, pH 7.5) and lysed by sonication. The lysate was clarified by centrifugation (23000 x g, 20 min, 4°C). The supernatant was applied to a gravity column with 2 ml GST resin (Macherey-Nagel), pre-equilibrated and washed with buffer A, eluted with buffer B1 (50 mM Tris, 150 mM NaCl, pH 8.0). The eluted protein was dialyzed against buffer C1 (50 mM Tris, 150 mM NaCl, 20mM GSH, pH 8.0) and cleaved by thrombin. The GST was separated from the peptides by a subsequent GST purification step. The H1 fragments were further purified by reverse-phase HPLC on a C-18 (Phenomenex) column by using a gradient of water/acetonitrile. Collected fractions were lyophilized and their identity was confirmed by using a Perkin–Elmer Sciex API2000 mass spectrometer.

Cell pellets containing the MBP-fused podocin fragments were lysed and clarified as described above. The supernatant was applied to a gravity column with 5 ml amylose resin pre-equilibrated and washed with buffer A, eluted with buffer B2 (50 mM Tris, 150 mM NaCl, 40 mM Maltose, pH 7.5). The eluted protein was dialysed against buffer C2 (50mM Tris, 50 mM NaCl, 1 mM DTT, pH 7.5) and subsequently an Q-IEX purification was performed by using a gradient of buffer D2 (50 mM Tris, 1 M NaCl, 1 mM DTT, pH 7.5). The eluted fraction was purified and subsequently analyzed by gel-filtration chromatography using buffer A (50 mM Tris, 50 mM NaCl, pH 7.5) with 10 µM of protein in buffer A. These purified MBP-fused podocin fragments were used to perform FRET experiments with 40 µM of protein in buffer A. Maleimide staining and FRET measurements were performed as described above.

Electronic Circular Dichroism Spectroscopy

Far-UV ECD spectra were recorded on a Jasco J810 spectrophotometer using cuvettes with a path length of 1.0 mm with protein concentrations of 40 µM. Typical spectral accumulation parameters were a scan rate of 50 nm/min with a 1 nm bandwidth and a 0.2 nm step resolution over wavelength ranges of 185–260 nm (far-UV) with four scans averaged for each spectrum. The temperature at the cell was controlled by a Peltier-type heating system. The solvent reference spectra were used as baselines that were automatically subtracted from the peptide spectra. The raw ellipticity data were converted into mean residue molar ellipticity units ($[\Theta]_{MR}$, degrees square centimeters per decimole).

Expression of podocin variants in podocytes

A human immortalized podocyte cell line (AB8/13) provided by M. Saleem (University of Bristol, UK) [43] was cultured at 33°C in RPMI-1640 supplemented with 10% FBS, insulin-transferrin-selenium (Life Technologies), and 50 IU/ml penicillin/streptomycin (Life Technologies). The podocytes do not express endogenous podocin and remain undifferentiated at this growth-permissive temperature [43]. Cells were tested for mycoplasma contamination every 3 months. Podocytes were cultured on type I collagen-coated coverslips and cotransfected with plasmids encoding HA-podocin or podocin-GFP variants using FuGENE HD according to the manufacturer's instructions (Promega). To assess the colocalization of podocin and internalized transferrin, podocytes were washed after 24 hrs of transfection, and pre-incubated with serum-free and insulin-transferrin-selenium free RPMI-1640 for 1 hr at 33°C. Then, cells were incubated with 8 µg/ml of Alexa594-conjugated transferrin (Life Technologies), in serum-free medium for 1 hr at 4°C. Cells were washed with PBS, then placed at 33°C for 10 min to let the transferrin internalize, washed with PBS twice and fixed in 4% formaldehyde. After washing, cells were treated with 50 mM NH_4Cl and incubated with a blocking solution (PBS, 1% BSA, 0.1% Tween20) for 1 hr prior to primary antibody hybridization then with appropriate Alexa Fluor-conjugated secondary antibodies (Life Technologies). Nuclei were stained with Hoechst (Life Technologies). To assess the effect of dynamin on HA-podocin variants internalization, GFP-fused wild-type or dominant negative mutant (K44A) dynamin [27] was co-expressed with HA-podocin variants in podocytes.

Analysis of the subcellular localization of podocin

Transfected podocytes were incubated with Alexa Fluor 555-conjugated wheat germ agglutinin (WGA; Life technologies) for 20 min at 4°C to stain plasma membrane, then fixed with ice-cold ethanol for 5 min. Fixed cells were blocked with PBS/BSA 1% for 15 min and incubated with mouse anti-HA primary antibodies (Covance) followed by Alexa Fluor 647-conjugated secondary antibodies (Life technologies). Confocal optical slices were captured using a 40x oil objective lens (Leica

Microsystems), an optical slice thickness of 800 nm, a Z-step size of 250 nm and XY pixel size of 86 nm (Leica SP8 confocal microscope, Necker Imaging Facility). The perimembranous region was defined by delimitating WGA-labeled membrane extensions using ImageJ 1.51k software. The membrane-targeting of podocin proteins was characterized by the ratio of the WGA-labeled perimembranous area which colocalized with podocin, and was quantified as the Manders' coefficient, calculated by ImageJ.

Statistical analysis

FRET efficiencies were compared by ANOVA and Tukey HSD post-hoc test. The fraction of plasma membrane overlapping podocin was compared using Kruskal-Wallis test followed, if significant, by Multiple comparisons of mean ranks. Renal survival in patients with R286Tfs*17 and A317Lfs*31 mutations was compared by log-rank test. The effect of dynamin on the membrane localization of podocin variants was assessed by Mann-Whitney U test. Correlation between the membrane localization of coexpressed podocin variants was tested by Pearson correlation. All statistical analyses were performed by Statistica software version 13.2.

Disclosure

The authors declare no competing financial interest.

References

1. Boute N, Gribouval O, Roselli S, et al. NPHS2, encoding the glomerular protein podocin, is mutated in autosomal recessive steroid-resistant nephrotic syndrome. *Nat Genet.* 2000;24(4):349-354.
2. Machuca E, Benoit G, Nevo F, et al. Genotype-phenotype correlations in non-Finnish congenital nephrotic syndrome. *J Am Soc Nephrol.* 2010;21(7):1209-1217.
3. Hinkes BG, Mucha B, Vlangos CN, et al. Nephrotic syndrome in the first year of life: two thirds of cases are caused by mutations in 4 genes (NPHS1, NPHS2, WT1, and LAMB2). *Pediatrics.* 2007;119(4):e907-919.
4. Santin S, Bullich G, Tazon-Vega B, et al. Clinical Utility of Genetic Testing in Children and Adults with Steroid-Resistant Nephrotic Syndrome. *Clin J Am Soc Nephrol.* 2011.
5. Sadowski CE, Lovric S, Ashraf S, et al. A single-gene cause in 29.5% of cases of steroid-resistant nephrotic syndrome. *J Am Soc Nephrol.* 2015;26(6):1279-1289.
6. Schwarz K, Simons M, Reiser J, et al. Podocin, a raft-associated component of the glomerular slit diaphragm, interacts with CD2AP and nephrin. *J Clin Invest.* 2001;108(11):1621-1629.
7. Roselli S, Gribouval O, Boute N, et al. Podocin localizes in the kidney to the slit diaphragm area. *Am J Pathol.* 2002;160(1):131-139.
8. Huber TB, Simons M, Hartleben B, et al. Molecular basis of the functional podocin-nephrin complex: mutations in the NPHS2 gene disrupt nephrin targeting to lipid raft microdomains. *Hum Mol Genet.* 2003;12(24):3397-3405.
9. Huber TB, Kottgen M, Schilling B, Walz G, Benzing T. Interaction with podocin facilitates nephrin signaling. *J Biol Chem.* 2001;276(45):41543-41546.
10. Tossidou I, Teng B, Drobot L, et al. CIN85/RukL is a novel binding partner of nephrin and podocin and mediates slit diaphragm turnover in podocytes. *J Biol Chem.* 2010;285(33):25285-25295.
11. Kim EY, Anderson M, Wilson C, Hagmann H, Benzing T, Dryer SE. NOX2 interacts with podocyte TRPC6 channels and contributes to their activation by diacylglycerol: essential role of podocin in formation of this complex. *Am J Physiol Cell Physiol.* 2013;305(9):C960-971.
12. Huber TB, Schermer B, Muller RU, et al. Podocin and MEC-2 bind cholesterol to regulate the activity of associated ion channels. *Proc Natl Acad Sci U S A.* 2006;103(46):17079-17086.
13. Reiser J, Polu KR, Moller CC, et al. TRPC6 is a glomerular slit diaphragm-associated channel required for normal renal function. *Nat Genet.* 2005;37(7):739-744.
14. Exome Variant Server NGESPE. Seattle, WA (URL: http://evs.gs.washington.edu/EVS/).
15. Tsukaguchi H, Sudhakar A, Le TC, et al. NPHS2 mutations in late-onset focal segmental glomerulosclerosis: R229Q is a common disease-associated allele. *J Clin Invest.* 2002;110(11):1659-1666.
16. Tonna S, Wang YY, Wilson D, et al. The R229Q mutation in NPHS2 may predispose to proteinuria in thin-basement-membrane nephropathy. *Pediatr Nephrol.* 2008;23(12):2201-2207.
17. Voskarides K, Arsali M, Athanasiou Y, Elia A, Pierides A, Deltas C. Evidence that NPHS2-R229Q predisposes to proteinuria and renal failure in familial hematuria. *Pediatr Nephrol.* 2012;27(4):675-679.
18. Kerti A, Csohany R, Wagner L, Javorszky E, Maka E, Tory K. NPHS2 homozygous p.R229Q variant: potential modifier instead of causal effect in focal segmental glomerulosclerosis. *Pediatr Nephrol.* 2013;28(10):2061-2064.
19. Tory K, Menyhard DK, Woerner S, et al. Mutation-dependent recessive inheritance of NPHS2-associated steroid-resistant nephrotic syndrome. *Nat Genet.* 2014;46(3):299-304.
20. Lipska BS, Balasz-Chmielewska I, Morzuch L, et al. Mutational analysis in podocin-associated hereditary nephrotic syndrome in Polish patients: founder effect in the Kashubian population. *J Appl Genet.* 2013;54(3):327-333.

21. Dosztanyi Z, Csizmok V, Tompa P, Simon I. IUPred: web server for the prediction of intrinsically unstructured regions of proteins based on estimated energy content. *Bioinformatics.* 2005;21(16):3433-3434.
22. Drozdetskiy A, Cole C, Procter J, Barton GJ. JPred4: a protein secondary structure prediction server. *Nucleic Acids Res.* 2015;43(W1):W389-394.
23. Yokoyama H, Fujii S, Matsui I. Crystal structure of a core domain of stomatin from Pyrococcus horikoshii Illustrates a novel trimeric and coiled-coil fold. *J Mol Biol.* 2008;376(3):868-878.
24. Godel M, Ostendorf BN, Baumer J, Weber K, Huber TB. A novel domain regulating degradation of the glomerular slit diaphragm protein podocin in cell culture systems. *PLoS One.* 2013;8(2):e57078.
25. Greenfield NJ. Using circular dichroism spectra to estimate protein secondary structure. *Nat Protoc.* 2006;1(6):2876-2890.
26. Hinkes B, Vlangos C, Heeringa S, et al. Specific podocin mutations correlate with age of onset in steroid-resistant nephrotic syndrome. *J Am Soc Nephrol.* 2008;19(2):365-371.
27. van der Bliek AM, Redelmeier TE, Damke H, Tisdale EJ, Meyerowitz EM, Schmid SL. Mutations in human dynamin block an intermediate stage in coated vesicle formation. *J Cell Biol.* 1993;122(3):553-563.
28. McCarthy HJ, Bierzynska A, Wherlock M, et al. Simultaneous sequencing of 24 genes associated with steroid-resistant nephrotic syndrome. *Clin J Am Soc Nephrol.* 2013;8(4):637-648.
29. He N, Zahirieh A, Mei Y, et al. Recessive NPHS2 (Podocin) mutations are rare in adult-onset idiopathic focal segmental glomerulosclerosis. *Clin J Am Soc Nephrol.* 2007;2(1):31-37.
30. Roselli S, Moutkine I, Gribouval O, Benmerah A, Antignac C. Plasma membrane targeting of podocin through the classical exocytic pathway: effect of NPHS2 mutations. *Traffic.* 2004;5(1):37-44.
31. Snyers L, Umlauf E, Prohaska R. Oligomeric nature of the integral membrane protein stomatin. *J Biol Chem.* 1998;273(27):17221-17226.
32. Rungaldier S, Umlauf E, Mairhofer M, Salzer U, Thiele C, Prohaska R. Structure-function analysis of human stomatin: A mutation study. *PLoS One.* 2017;12(6):e0178646.
33. Umlauf E, Mairhofer M, Prohaska R. Characterization of the stomatin domain involved in homo-oligomerization and lipid raft association. *J Biol Chem.* 2006;281(33):23349-23356.
34. Lee A, Frank DW, Marks MS, Lemmon MA. Dominant-negative inhibition of receptor-mediated endocytosis by a dynamin-1 mutant with a defective pleckstrin homology domain. *Curr Biol.* 1999;9(5):261-264.
35. Sasaki Y, Hidaka T, Ueno T, et al. Sorting Nexin 9 facilitates podocin endocytosis in the injured podocyte. *Sci Rep.* 2017;7:43921.
36. Kerti A, Csohany R, Szabo A, et al. NPHS2 p.V290M mutation in late-onset steroid-resistant nephrotic syndrome. *Pediatr Nephrol.* 2012.
37. Weber S, Gribouval O, Esquivel EL, et al. NPHS2 mutation analysis shows genetic heterogeneity of steroid-resistant nephrotic syndrome and low post-transplant recurrence. *Kidney Int.* 2004;66(2):571-579.
38. Bouchireb K, Boyer O, Gribouval O, et al. NPHS2 mutations in steroid-resistant nephrotic syndrome: a mutation update and the associated phenotypic spectrum. *Hum Mutat.* 2014;35(2):178-186.
39. Suvanto M, Patrakka J, Jahnukainen T, et al. Novel NPHS2 variant in patients with familial steroid-resistant nephrotic syndrome with early onset, slow progression and dominant inheritance pattern. *Clin Exp Nephrol.* 2016.
40. Shen N, Heintz C, Thiel C, Okun JG, Hoffmann GF, Blau N. Co-expression of phenylalanine hydroxylase variants and effects of interallelic complementation on in vitro enzyme activity and genotype-phenotype correlation. *Mol Genet Metab.* 2016;117(3):328-335.

41. Rodriguez-Pombo P, Perez-Cerda C, Perez B, Desviat LR, Sanchez-Pulido L, Ugarte M. Towards a model to explain the intragenic complementation in the heteromultimeric protein propionyl-CoA carboxylase. *Biochim Biophys Acta.* 2005;1740(3):489-498.
42. Kitamura A, Tsukaguchi H, Maruyama K, et al. Steroid-resistant nephrotic syndrome. *Kidney Int.* 2008;74(9):1209-1215.
43. Saleem MA, O'Hare MJ, Reiser J, et al. A conditionally immortalized human podocyte cell line demonstrating nephrin and podocin expression. *J Am Soc Nephrol.* 2002;13(3):630-638.

Acknowledgements

We thank Mária Bernáth for the technical assistance. We greatly acknowledge Meriem Garfa-Traoré and Nicolas Goudin of the Cell Imaging Platform at Imagine Institute for providing expert knowledge on confocal microscopy. Human immortalized podocytes were kindly provided by M. Saleem (Bristol Royal Hospital for Children, University of Bristol, UK). Financial support for this work was provided by MTA-SE Lendulet Research Grant (LP2015-11/2015) of the Hungarian Academy of Sciences, NKFIA/OTKA K109718, K116305, KH125566, MedinProt Synergy grant (DKM, SP and TK), State funding from the Agence Nationale de la Recherche under "Investissements d'avenir" program (ANR-10-IAHU-01), EURenOmics (the European Community's 7th Framework program grant 2012-305608), the Agence Nationale de la Recherche (GenPod project ANR-12-BSV1-0033.01), Eotvos Scholarship of the Hungarian State (KT) and by the French-Hungarian bilateral project (PHC 34501SM Balaton, Hungarian Grant No. TeT_14_1-2015-0020).

Author contributions

KT, GM, PS, GS, CAn, DKM, AB, AP designed the study. CAr performed the mutagenesis and the expression experiments in podocytes. KT analyzed the membrane targeting of podocin. PS performed the bacterial expressions, ECD spectroscopy measurements and the size exclusion chromatography experiments. EB and AM produced the podocin variants for FRET measurements. GS and GL performed the FRET experiments. KT and GS made the statistical analyses. KT, GS, DKM, PS, EB and GM wrote the paper.